Journal of Inorganic and Organometallic Polymers and Materials (2023) 33:1855–1867
https://doi.org/10.1007/s10904-023-02622-y

RESEARCH

# Structural, Optical and Antibacterial Activity Studies on CMC/PVA Blend Filled with Three Different Types of Green Synthesized ZnO Nanoparticles

**A. Y. Yassin[1] · A. M. Abdelghany[2] · Reda S. Salama[3] · A. E. Tarabiah[4]**

Received: 13 February 2023 / Accepted: 17 March 2023 / Published online: 1 April 2023


**Abstract**
In this work, zinc oxide (ZnO) was produced using extracts of Thymus (Z), *Hibiscus rosa-sinensis* (K), and *Daucus carota* (G). Furthermore, sodium carboxymethyl cellulose (CMC) and polyvinyl alcohol (PVA) were combined with ZnO to form three novel nanocomposites. X-ray diffraction (XRD) was used for the structural analysis, where the semicrystalline nature of the (CMC/PVA)/ZnO nanocomposites was confirmed. The characteristics functional groups that arose inside the prepared samples were identified by Fourier transform infrared spectroscopy (FTIR). Evidence for the successful preparation of the pure ZnO particles and their nanocomposites was carried out using a transmission electron microscope (TEM). The ZnO nanoparticles are mostly spherical, irregularly distributed, and have radii ranging from 10 to 40 nm. Their anti-bacterial activity was studied against *B. subtilis*, *E. coli,* and *Candida albicans*. The inhibition zones of all the prepared samples against *E. coli* were 0, 19, 31, and 23 mm for PVA/CMC blend, PVA/CMC/ZnO (Z) (PCZ-Z), PVA/CMC/ZnO (K) (PCZ-K), and PVA/CMC/ZnO (G) (PCZ-G), respectively, compared to the streptomycin control Gram-positive standard with inhibition zone (34 mm). On the other hand, the inhibition zones of the prepared samples against *B. subtilis* were equal to 0, 26, 33, and 28 mm for CMC/PVA, PCZ-Z, PCZ-K, and PCZ-G, respectively. Based on these results, the PCZ-K sample is the most effective at resisting *E. coli* (91.17%) and *B. subtilis* (94.28%). These nanocomposites do not have harmful chemicals, making them strong candidates for use in biological applications.

**Keywords** CMC/PVA · ZnO nanoparticles · Plant extract · XRD · Antibacterial activity

## 1 Introduction

Nano-sized inorganic composites have exhibited extraordinary antibacterial activity at extremely low concentrations because of their exceptional physiochemical properties and high surface area-to-volume ratio [1, 2]. Moreover, these compounds are thermally stable at high pressure. Some of them are considered non-toxic and even contain vital minerals for the human body. Metal and metal oxide nanoparticles (NPs), like gold, copper, silver, zinc oxide, manganese oxide, and titanium oxide, were identified as the most antibacterial inorganic materials [3–5].

As nanotechnology advances, more and more attention is being paid to how nanomaterials affect bacteria and fungi, with the hope that this may lead to improved hygiene in public places [6]. One of the non-toxic nanomaterials that might be employed in biomedical applications is zinc oxide nanoparticles (ZnO NPs). They are effective against cancer and microbes [7].

Among the many benefits of ZnO are its good electrochemical features, wide absorption spectrum, and strong chemical stability. In addition to being beneficial for electrical and optoelectronic applications like storage devices and solar cells [8], its large energy bandwidth and thermal stability also qualify it as a semiconductor. Likewise, their

✉ A. Y. Yassin
a_yassin2200@yahoo.com

1 Department of Basic Sciences, Delta University for Science and Technology, Gamassa, Mansoura, Egypt

2 Spectroscopy Department, Physics Division, National Research Center, Dokki, Cairo, Egypt

3 Basic Science Department, Faculty of Engineering, Delta University for Science and Technology, Gamassa, Egypt

4 Dental Biomaterials Department, Faculty of Oral and Dental Medicine, Delta University for Science and Technology, Gamassa, Egypt

ability to absorb UV rays makes them an essential ingredient in enzymes, cosmetics, toothpaste, and sunscreens [9]. ZnO has piezoelectric and pyroelectric properties that make it useful for the development of sensors, generators, and photocatalysis. It has low toxicity and biocompatibility, facilitating its applications in biomedicine [10].

Several studies [11–13] have reported on the different techniques to synthesize ZnO nanoparticles and its modification over different blends. They also studied its biological activities, as reported by Nadeem et al. [11], where they studied the antimicrobial activity of iron (Fe) and cobalt (Co) co-doped ZnO nanoparticles and displayed an enhancement in antibacterial activity by co-doping with iron and cobalt. Moreover, Mukhtar et al. [12] reported the photocatalytic properties of titanium, vanadium, and yttrium oxides and showed an increase in photocatalytic activity by mixing them together, as well as displayed excellent antibacterial activities.

To avoid agglomeration and control excessive growth of nanoparticles, nanomaterials synthesized from organometallic precursors need the application of a capping agent that works as a stabilizer and makes colloids more stable [14]. The two most high-performance stabilizing agents are carboxymethyl cellulose (CMC) and polyvinyl alcohol (PVA) [15]. Hydrolysis of polyvinyl acetate yields PVA, a synthetic polymer with excellent biodegradability, biocompatibility, and hydrophilicity [16]. PVA is employed in different biological applications, where its hydrogels have significant potential for use in artificial grafts and tissue engineering. PVA is a low-cost, lightweight polymer with high mechanical and optical qualities that is also environmentally friendly. It can also be utilized in various industrial applications due to its superior chemical and physical qualities, such as textile sizing, solar cells, adhesives, soil stabilizers, surgical, optoelectronic, and biological devices [17, 18]. Additionally, one of the most important cellulose derivatives is carboxymethyl cellulose (CMC) which is treated with chloroacetic acid ($ClCH_2CO_2H$). It's utilized in the cosmetic, paints, pharmaceutics, mineral processing, food, textiles, ceramic foam, biodegradable films, and paper industries as a thickener, binder, suspension stabilizer (stabilizing agent), and water-retaining agent [19].

In the current study, zinc oxide (ZnO) nanoparticles were synthesized from Thymus (Z), *Hibiscus rosa-sinensis* (K), and *Daucus carota* (G) extracts. After that, ZnO NPs were combined with sodium carboxymethyl cellulose (CMC) and polyvinyl alcohol (PVA) to form three novel nanocomposites. The synthesized nanocomposites were investigated by different techniques, including TEM, XRD, UV–Vis, and FT-IR spectroscopy. The antibacterial activity of the prepared composites was studied against *B. subtilis*, *E. coli*, and *Candida albicans*.

## 2 Materials and Methods

### 2.1 Materials

Polyvinyl alcohol (PVA) purchased from Acros (USA) has a molecular weight ≈ 6000 g/mol. Carboxymethyl cellulose (CMC) supplied by Lanxess (Germany), in combination with Zinc acetate dehydrate ($Zn(CH_3COO)_2{\cdot}2H_2O$) as a precursor supplied by the Sigma Aldrich company.

### 2.2 Synthesis of ZnO Nanoparticles

Thyme (Z), *Hibiscus rosa-sinensis* (K), and *Daucus carota* (G) were rinsed using tap water, followed by double-distilled water and ethanol to remove any trace of contamination. The plants were then dried at room temperature. About 10 g of each plant was ground in an agate mortar. The obtained powder was mixed separately with 250 mL of distilled water adjusted at about 75 °C for 1 h. The mixture was then filtered using Whatman filter paper No. 1. The obtained solutions were stored in dark bottles at 4 °C. A 0.01 M aqueous solution of zinc acetate dihydrate ($Zn(CH_3COO)_2{\cdot}2H_2O$) was prepared and stored as a stock solution. 95 mL of the stoke solution was mixed with 5 mL of the plant extract, where each plant was in a separate flask. The resulting mixture was incubated for one hour at 75 °C while being continuously shaken at 150 rpm. As a result, bio-reduced salt ultimately settled in the flasks in the form of white precipitate. The supernatant was poured, and the precipitate was centrifuged and washed four times with deionized water to assure the elimination of contaminants [20].

#### 2.2.1 Preparation of the Polymer Blend and Its Nanocomposites

The preparation steps are shown in Scheme 1. In brief, 2 g of both polyvinyl alcohol (PVA) and carboxymethyl cellulose (CMC) were vigorously stirred individually in deionized water. The obtained solutions were then mixed for about 3 h until a clear, bubble-free mixture solution was obtained. The final mixture was then divided into four equal parts. The same quantity of ZnO nanoparticles synthesized from different plants, viz., thyme, rosella (*Hibiscus sabdariffa*), and carrots designated as shown in Table 1, was mixed with the blend sample using a sonicator homogenizer. Samples were then incubated at 50 °C for 2 days after being decanted into plastic Petri dishes to ensure evaporation of any solvent traces. The final product was in the form of thin films that were stored in a vacuum desecrator until use. Table 1 shows the symbols for the samples that were synthesized with different ZnO nanoparticles made from different plants.

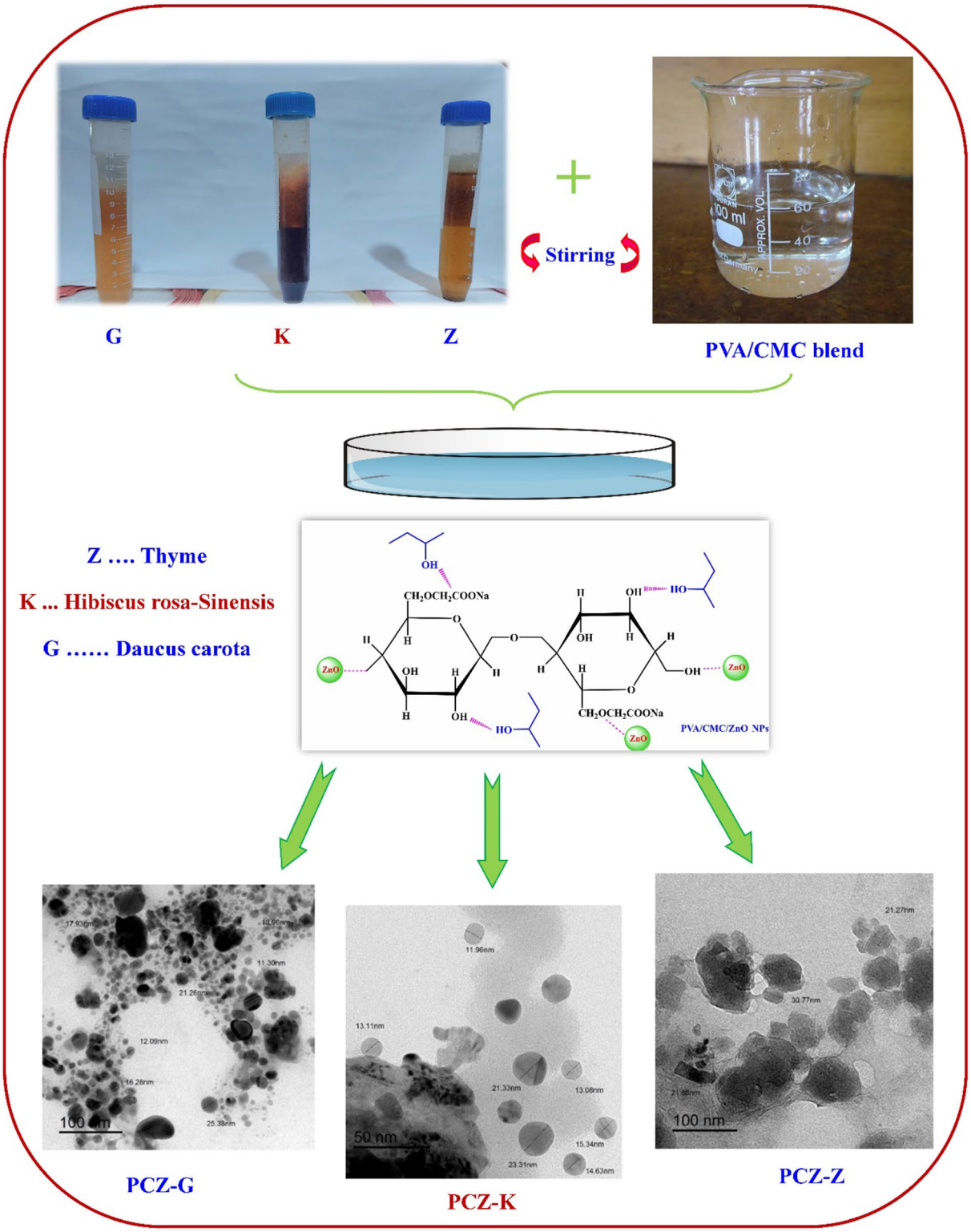


**Scheme 1** The preparation steps of the (CMC/PVA)/ZnO nanocomposites

**Table 1** Sample composition and designation

| Sample | Symbol | PVA (wt%) | CMC (wt%) | ZnO | Source |
|---|---|---|---|---|---|
| PVA/CMC blend | Pure blend | 50 | 50 | 0.0 | |
| PVA/CMC/ZnO (Z) | PCZ-Z | 49.95 | 49.95 | 0.1 | Thymus |
| PVA/CMC/ZnO (K) | PCZ-K | 49.95 | 49.95 | 0.1 | *Hibiscus rosa-sinensis* |
| PVA/CMC/ZnO (G) | PCZ-G | 49.95 | 49.95 | 0.1 | *Daucus carota* |

**Scheme 2** Molecular interaction of PVA and CMC

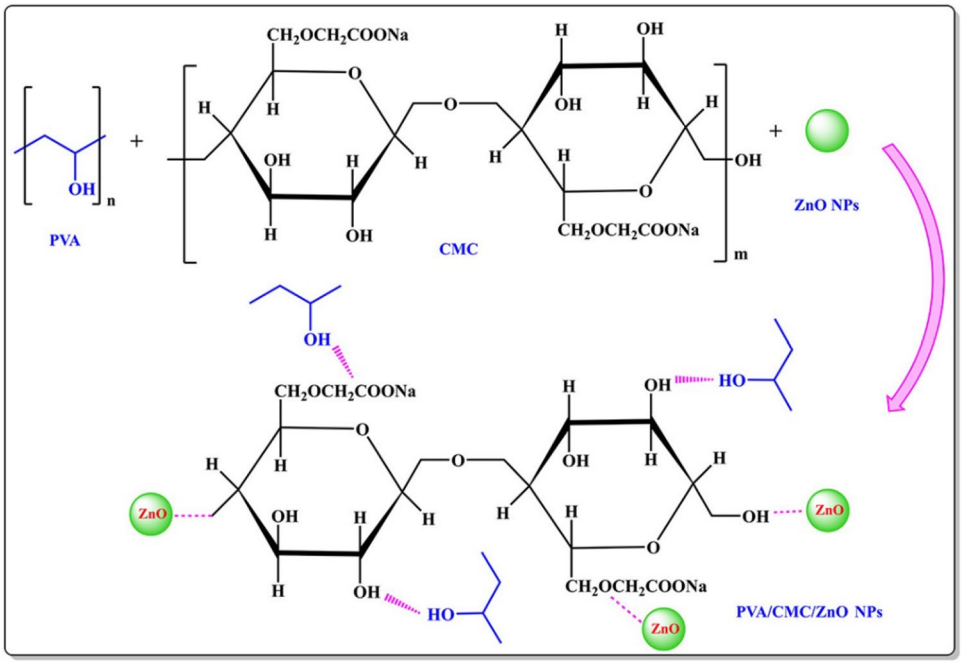


## 2.3 Measurements

### 2.3.1 Characterization of Polymer Nanocomposites

The molecular interaction between the nanocomposite constituents is exhibited in Scheme 2. The crystallinity of the prepared nanocomposite samples was examined through an X-ray diffractometer (X'Pert PRO) with Cu Kα radiation at 30 kV and a wavelength of 0.15406 nm in room temperature. The structural features of all samples were investigated using a Fourier transform infrared (FTIR) spectrometer (Nicolet iS10) in the spectral region of 4000 $cm^{-1}$ to 400 $cm^{-1}$. The prepared composites were coated on copper grids (200 mesh) and inspected by HRTEM (JEM-2100) at 200 kV for transmission electron microscopic examination to examine the particle size and morphology of the prepared nanocomposites. The optical properties of the prepared composites were tested using a spectrophotometer (V/570 UV/VIS–NIR, JASCO, Japan) in the range of 200–1100 nm.

### 2.3.2 Evaluation of Antibacterial Activity

Usually, the antibacterial activities of the present composites were estimated by the disc diffusion technique using inoculums consisting of $10^6$ bacterial spreads on Mueller–Hinton agar plates [21]. The activities of *Bacillus subtilis* as Gram-positive bacteria, *Escherichia coli* as Gram-negative bacteria, and *Candida albicans* as fungi were examined for the synthesized samples by the qualitative technique. 20 mL of Mueller agar was placed into sterile petri dishes, allowed to harden, and then dried in the incubator. A total of roughly $10^6$ cells were spread out on the agar plate using a sterilized glass rod, and the plate was then allowed to dry to a standard turbidity of 0.5 McFarland. The discs of samples were placed on top of agar plates that had been planted. The agar plates were incubated for one day at 37 °C. Each plate was tested after incubation. For each bacterium, positive control of streptomycin (100 mg/mL) is utilized. The disc's diameter as well as the diameter of the inhibition zones were measured. Zones are measured to the closest full millimeter

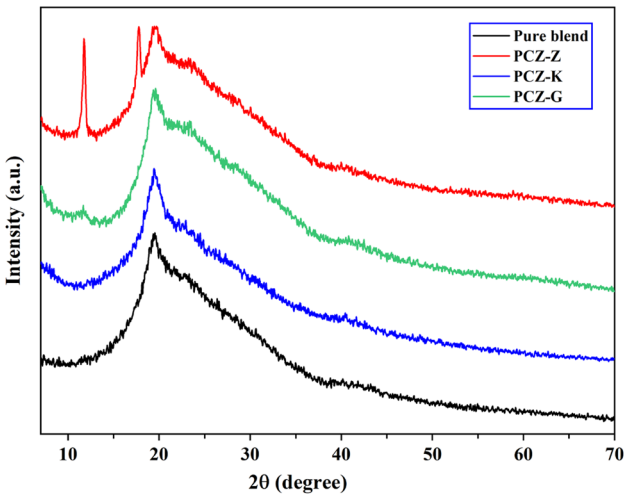


**Fig. 1** XRD spectra of CMC/PVA blend doped with ZnO-NPs extracted from three different plants

using calipers or a ruler placed on the back of the upright petri dish.

## 3 Results and Discussion

### 3.1 XRD Analysis

The XRD spectra of the CMC/PVA blend doped with ZnO-NPs extracted from the three different plants are displayed in Fig. 1. For the pure PVA/CMC blend, the protuberant broad peak at $2\theta \approx 19.35°$ was ascribed to the semicrystalline nature of PVA [22] and the crystalline cellulosic structure [18]. The other peak, centering at $2\theta \approx 41.13°$, indicates the presence of a representative semi-crystalline structure, suggesting that CMC interacted strongly with PVA [23]. The first broad peak has shifted with the addition of ZnO nanoparticles, confirming the efficacy and compatibility of the ZnO-based filler in the polymer blend matrix. Some parameters, such as area under the main peaks ($A_P$), d-spacing, and the full width at half maximum (FWHM), were calculated and listed in Table 2. The average crystalline size ($D_{cry}$) was determined by using Sherrer's method that was previously discussed in detail in the literature [24–26].

From this table, it is observed that the broadness of the main peak had increased, which could be due to the lattice strain in the nanocomposites [27]. Further, the degree of crystallinity ($X_{cry}$ %) was calculated using the Hermans–Weidinger approach [24]. The decrease in $X_{cry}$ % indicates that the amorphous areas were distributed throughout the host matrices, revealing that CMC/PVA/ZnO nanocomposites are semicrystalline in nature. The sharp peaks shown at $2\theta \approx 11.71°$ for the PCZ-G sample, and at $\theta \approx 11.77°$ and 17.81° for the PCZ-Z sample may be stemmed from the presence of ZnO-nanoparticles, confirming the above results and recommending them for use in advanced technological applications.

### 3.2 ATR-FTIR Spectroscopy

At room temperature, FT-IR spectroscopy was used to look at how the molecules in the current blend interacted with each other and with the nanoparticles. The FT-IR spectra of pure and modified CMC/PVA blends with ZnO-NPs extracted from three different plants were demonstrated in Fig. 2. The figure displayed that all the prepared samples have characteristic bands such as; 3369 $cm^{-1}$ (O–H stretching of CMC or physically adsorbed water) [28, 29], 2928 $cm^{-1}$ ($CH_2$ asymmetrical str.), 1644 $cm^{-1}$ (C=O str.)

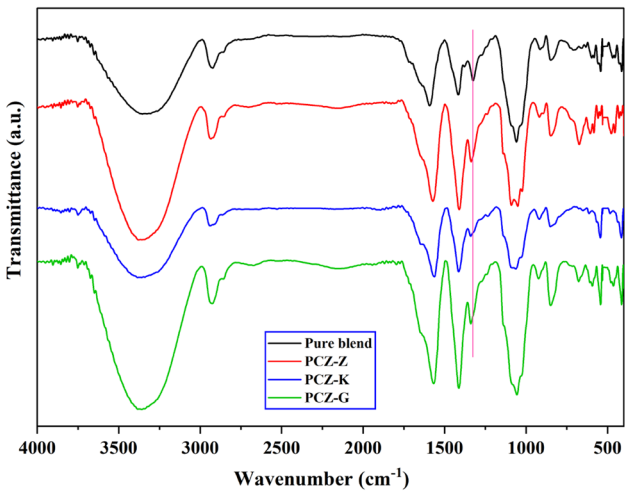


**Fig. 2** FT-IR spectra of the PVA/CMC polymer blend and the blend doped with ZnO-NPs extracted from three different plants

**Table 2** The Area under the peak ($A_P$), FWHM, $X_{cry}$ %, d-spacing, average crystalline size ($D_{cry}$), Urbach Energy (ΔE) and the indirect and direct optical energy gap values for the prepared samples

| Sample | $A_P$ | FWHM | $X_{Cry}$ % | d-spacing | $D_{cry}$ (nm) | $E_{igd}$ (eV) | $E_{gd}$ (eV) | ΔE (eV) |
|---|---|---|---|---|---|---|---|---|
| Pure blend | 13,620 | 12.44 | 39.08 | 4.49753 | – | 4.35 | 5.78 | 1.22 |
| PCZ-Z | 14,793 | 14.12 | 17.1 | 4.49787 | 10.8 | 4.25 | 5.50 | 1.00 |
| PCZ-K | 14,282 | 11.31 | 30.34 | 4.55624 | 13.58 | 3.52 | 4.80 | 1.16 |
| PCZ-G | 16,597 | 13.78 | 31.49 | 4.5153 | 11.15 | 4.00 | 5.22 | 0.97 |

**Table 3** Bands assignments for the FT-IR spectra of the prepared films under study

| Wavenumber ($cm^{-1}$) | Band assignment | Source |
|---|---|---|
| 3369 | –OH stretching | PVA + CMC |
| 2928 | $CH_2$ asymmetrical stretching | CMC |
| 1644 | C=O stretching (shoulder) | CMC |
| 1420 | –$CH_2$ scissoring | CMC |
| 1588 | Asymmetric carboxylate (–$COO^-$) str | CMC |
| 2857 | $CH_2$ symmetrical stretching | PVA |
| 1323 | –OH bending | CMC + PVA |
| 1057 | C-O str | PVA |
| 849 | –CH rocking | PVA |

[30], and 849 $cm^{-1}$ (C–H rocking of PVA) [31]. Table 3 summarizes additional band assignments for the FTIR spectra of the produced samples. The presence of oxygen in the ether bond allows hydrogen to interact with other molecules in the PVA and CMC polymers, leading to the development of a strong peak at 1092 $cm^{-1}$ [32]. This peak substantiates that the currently available nanocomposite samples have a semicrystalline structure. Furthermore, the intra-molecular interaction between the asymmetric carboxylate (–$COO^-$) str. groups and the bending hydroxyl groups (–OH) is responsible for the two spectral bands seen at 1588 $cm^{-1}$ and about 1323 $cm^{-1}$ [33]. Having these two functional groups improves the structural characteristics of the nanocomposites formed from ZnO-NPs and the CMC/PVA blend [34]. Similar CMC characteristic bands at 1581, 1421, 1334, and 1056 $cm^{-1}$, which were carbohydrate signature peaks, have been observed by previous reports [23, 35], indicating the existence of carboxymethyl substituents on the CMC backbone [36]. The observed shift in some peaks, such as –OH bending from 1323 to 1343 $cm^{-1}$ proves the constructive interaction of the current blend with ZnO NPs [37]. According to the available literature, the typical FT-IR bands of oxides are located between 600 and 400 $cm^{-1}$. Thus, the vibrational bands observed in the range of 600–400 $cm^{-1}$ correspond to the characteristic ZnO-NPs stretching vibrations [26]. The enhanced structural characteristics of the nanocomposite samples are further supported by the increased -OH band intensity, which shows the formation of hydrogen bonds.

### 3.3 UV/Vis Study

Absorbance spectrum data of the prepared samples in the ultraviolet and visible regions were illustrated in Fig. 3. The $\pi \rightarrow \pi^*$ transition is responsible for the 200 nm absorption edge in the UV region of the CMC/PVA mixture spectra [18]. After being filled with ZnO-NPs, the absorbance

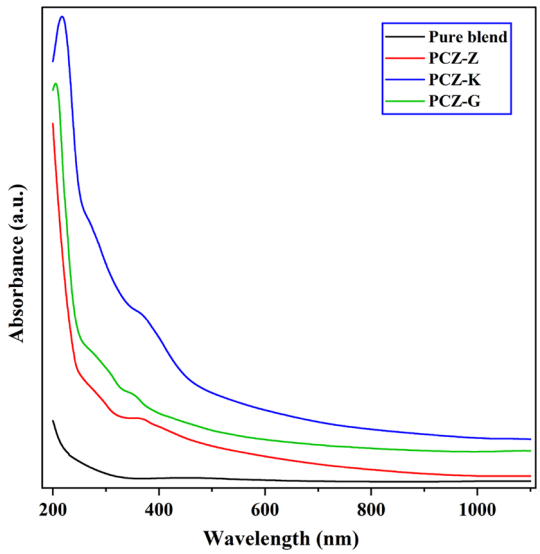


**Fig. 3** UV/VIS absorbance spectra for pure and filled CMC/PVA blend with ZnO-NPs extracted from the three different plants

values of the produced composites significantly increase, and a new absorption peak appears at about 350 nm. The presence of such a peak and its shift could be ascribed to the complexation and interaction behavior of the ZnO-NPs with polymeric matrices, affecting the optical band gap's value [38], which was associated with crystallinity variation in the nanocomposite, supporting the XRD findings [39]. The value of the optical energy gap ($E_g$) could be determined by the equation of Mott and Davis [40], which analyzes the spectrum dependency of the absorption coefficient near the absorption edge.

$$\alpha = \frac{B(h\upsilon - E_g)^m}{h\upsilon} \quad (1)$$

where B is an electronic transition probability constant and hυ is the energy of the incident photons. *m* is equivalent to 2 or 1/2 for the allowed direct and indirect transitions, respectively.

Figure 4 displays $(\alpha h\upsilon)^2$ and $(\alpha h\upsilon)^{1/2}$ plots of versus photon energy (hυ) of the as-synthesized composites. Linear extrapolation of these data points along the hυ axis yielded the optical band gap values shown in Table 2. The predicted optical energy gap reduces when ZnO-NPs are filled; this is ascribed to the function of ZnO-NPs in modifying the structural properties due to the development of varying polarons and defect contents, which are associated with the density of localized states N(E) [41]. Spectral measurements showed an extended tail that coincides with localised states in the valence band tail. The tail is longer because of ZnO-NPs defects, which allow it to reach into the conduction band at lower energies below the main edge. Therefore, the Urbach

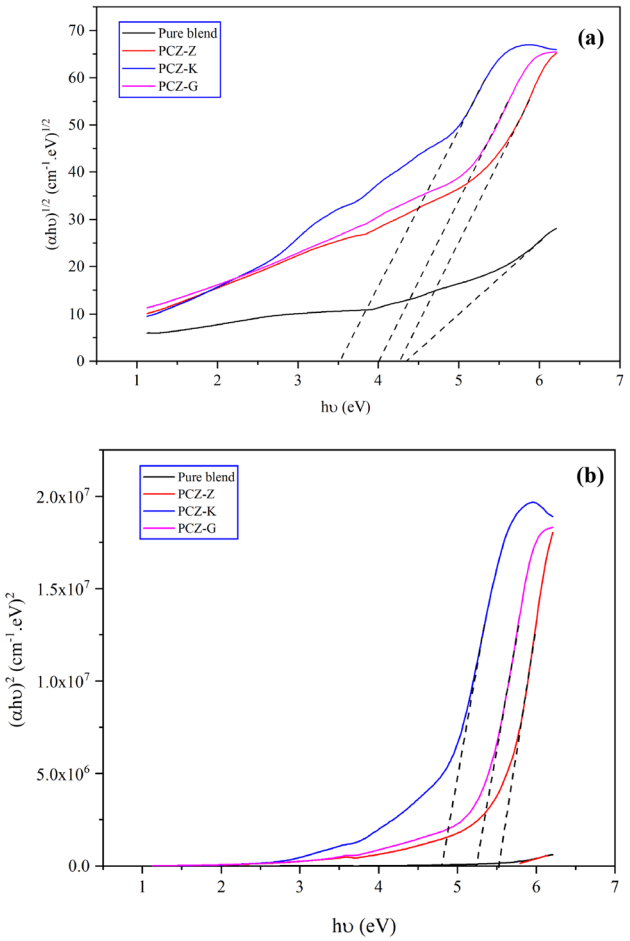


**Fig. 4** The plots of **a** $(\alpha h\upsilon)^{1/2}$, and **b** $(\alpha h\upsilon)^2$ versus $(h\upsilon)$ for pure and filled CMC/PVA blend with ZnO-NPs extracted from the three different plants

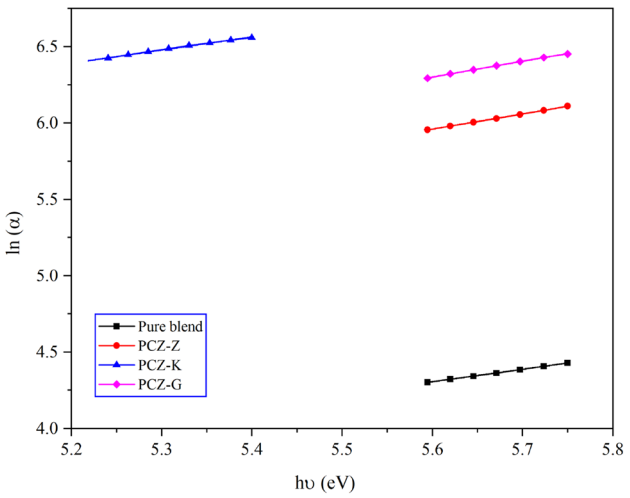


**Fig. 5** Absorption efficiency (α) of a CMC/PVA blend including ZnO-NPs as a function of photon energy (hυ)

formula [39] may be used to calculate the absorption coefficient (α) using just the energy tail width (ΔE) and the photon energy, both of which are correlated to thermal vibration in the lattice [22].

$$\alpha = \alpha_o exp\left(\frac{h\upsilon}{\Delta E}\right) \quad (2)$$

where $\alpha_o$ is a constant

Urbach energy values (ΔE) were calculated using Fig. 5's absorption coefficient-photon energy relationship. The ΔE values have been recorded in Table 2. The value of ΔE for the pure blend is 1.22 eV, whereas the filled samples have values ranging from 1.16 and 0.97 eV.

### 3.4 Transmission Electron Microscopy (TEM)

The morphology, nanoparticle size, and shape of the produced ZnO-NPs were checked using TEM images. Figure 6 displays TEM images for the purely obtained ZnO-NPs extracted from the three different plants and also shows the ZnO-NPs distributed in the aqueous solution of the CMC/PVA blend. The nanomaterials are mostly spherical, irregularly distributed, and their radii ranged from 10 to 40 nm. As well as, the images revealing that after addition of the CMC/PVA blend, the ZnO NPs were well dispersed over the blend, especially PCZ-K, which could have an excellent feature in the microbial activity. According to the nanoparticle size distribution histograms shown in Fig. 7, the average sizes of ZnO extracted from the three different plants were found to be 25.4, 15.2, and 17.9 nm for blended PCZ-G, PCZ-K, and PCZ-Z, respectively. So, the PCZ-K sample has the smallest particle size, which could affect the catalytic activity toward the different microbial organisms.

### 3.5 Antibacterial Activity

Figure 8 displays the antibacterial activity of CMC/PVA, PCZ-Z, PCZ-K and PCZ-G nanocomposites against *B. subtilis*, *E. coli*, and *Candida albicans*. The inhibition zone diameter was given in millimeters on the agar plate and calculated as an average value after each sample was repeated three times. The results are listed in Table 4. CMC/PVA did not display any antibacterial or antifungal activities. On the other hand, PCZ-Z, PCZ-K and PCZ-G displayed good antibacterial activity. The inhibition zone was bigger in *Hibiscus sabdariffa* than in *Daucus carota* and the thymus, which was interesting. These antibacterial activities for ZnO samples may result from numerous recommended mechanisms; the first mechanism is due to the size of nanoparticles of ZnO; when the particle size was decreased, the antibacterial activity was increased because of the concentration was increased [42]. The second process might include the introduction of $Zn^{2+}$ ions

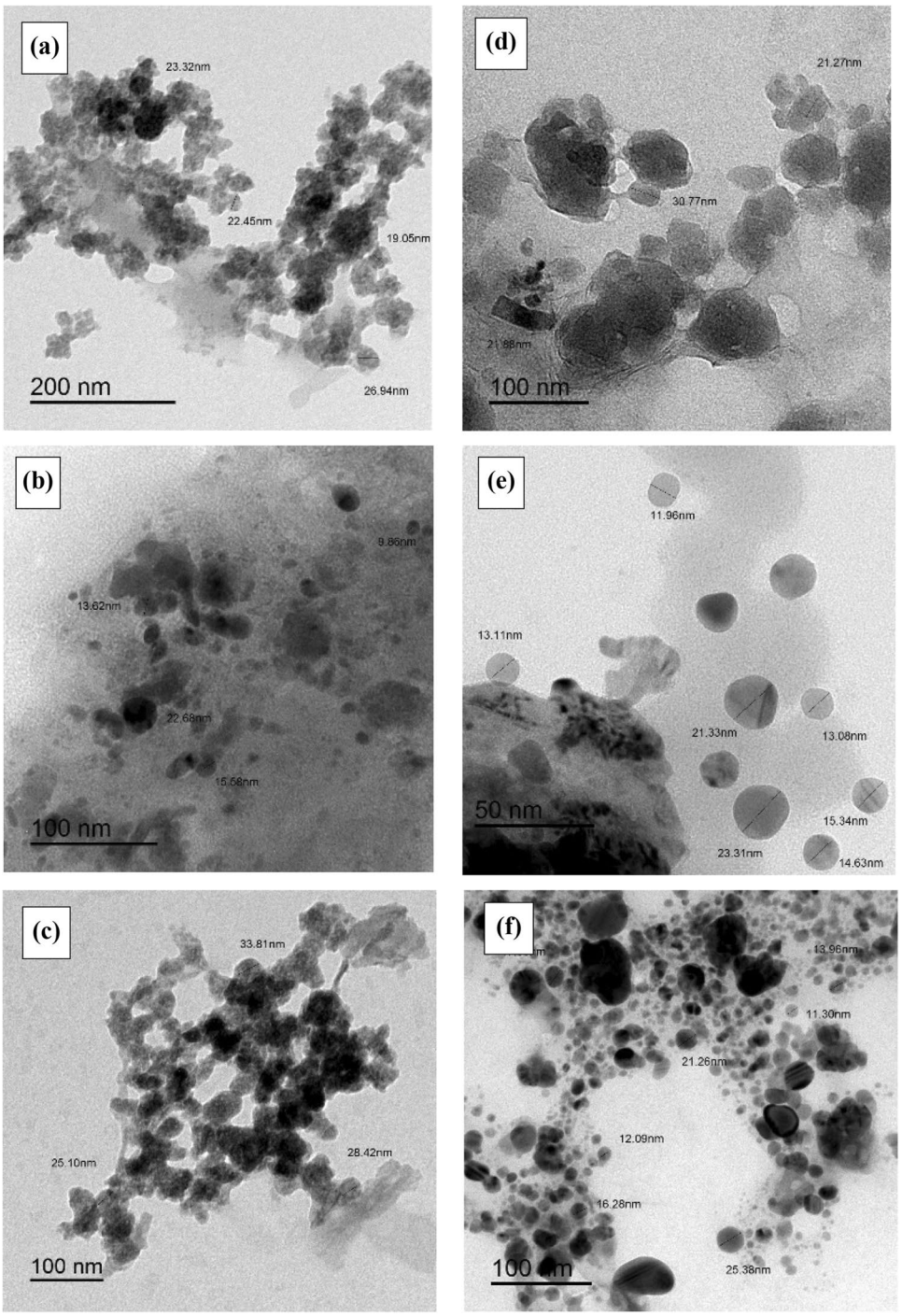


**Fig. 6** TEM Images of **a** pure synthesized ZnO-NPs (G), **b** pure synthesized ZnO-NPs (K), **c** pure synthesized ZnO-NPs (Z), **d** blended PCZ-G, **e** PCZ-K, and **f** PCZ-Z

into the bacterial growth medium [43, 44]. So, all the samples containing ZnO-NPs displayed excellent antibacterial activity and showed a deadly effect on the tested bacteria. The inhibition zones of all the prepared samples against *E. coli* was 0, 19, 31, and 23 mm for CMC/PVA, PCZ-Z, PCZ-K and PCZ-G, respectively, compared to the streptomycin control gram-positive standard with inhibition zone (34 mm). On the other hand, the inhibition zones of the prepared samples against *B. subtilis* were equal to 0, 26, 33, and 28 for CMC/PVA, PCZ-Z, PCZ-K and PCZ-G, respectively. These results reveal that PCZ-K sample has the maximum antibacterial efficiency for *E. coli* (91.17%) and *B. subtilis* (94.28%). Unfortunately, all the prepared samples have no activity toward *Candida albicans*, which means these samples do not have any antifungal activities. The improved antibacterial activity may be related to the CMC/PVA support that prevents the accumulation of ZnO nanoparticles and surface defects in ZnO [45].

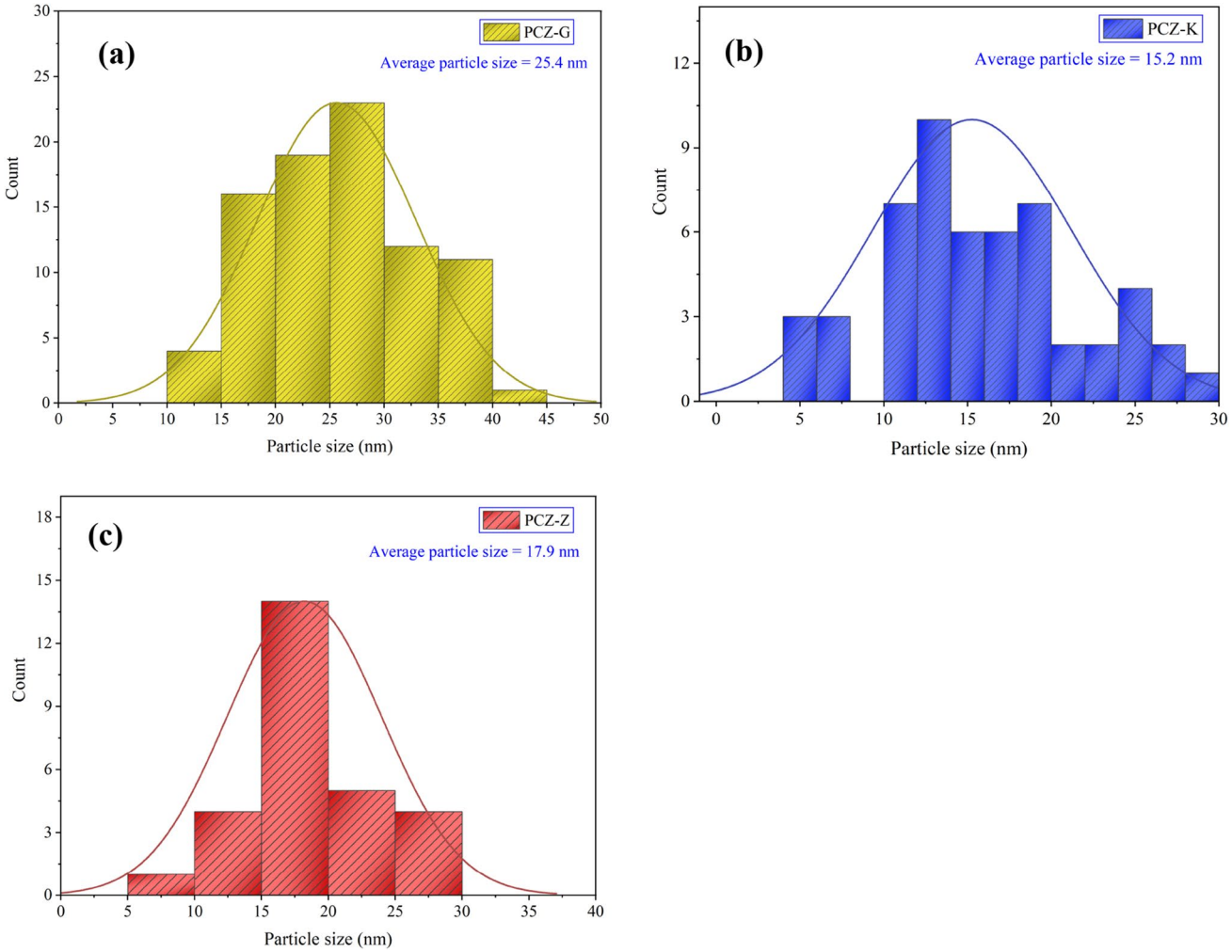


**Fig. 7** Nanoparticle size distribution histograms of **a** PCZ-G, **b** PCZ-K, and **c** PCZ-Z

The higher antibacterial activity of ZnO NPs could be related to the production of reactive oxygen species and the accumulation on the surface or deposition in the cytoplasm of the cells, as detected in the previous results for *S. aureus* [43]. The smallest particle size of 15.2 nm in the case of PCZ-K has been found to strongly inhibit the survival of pathogenic microorganisms tested compared with other results. So, the inhibitory efficacy of ZnO NPs is very much dependent on their size, which is similar to other findings [46].

The mechanisms of antibacterial activity of ZnO particles are not well understood, although some statements were proposed, such as the binding of ZnO particles on bacterial surfaces due to the electrostatic forces could be a mechanism [47], the generation of hydrogen peroxide could be the main factor of antibacterial activity [48], or the production of reactive oxygen species, that elevate membrane lipid peroxidation, which causes membrane leakage of reducing sugars, DNA, proteins, and reduces cell viability [49]. Herein, $Zn^{2+}$ ions collide with the cell membrane of bacteria having a negative charge. These electrostatic collision of positive $Zn^{2+}$ ions and negative cell membrane may prevent bacterial evolution. So, microbes are feeble that can weaken successively with time. Also, the creation of reactive oxygen species (ROS), including $H_2O_2$, $OH^*$, and $O^{2*-}$ played a crucial character in antibacterial sensation. The $O^{2*-}$, $OH^-$ being negatively charged, may stick to the material's surface and can damage DNA [50].

## 4 Conclusions

Pure and doped CMC/PVA blends with ZnO-NPs films were synthesized by the casting method using water as a solvent. The prepared composites were characterized by XRD, FTIR, TEM, and UV/Vis spectroscopy. UV/Vis and FTIR spectroscopy showed the complexation and interaction of both polymers and/or ZnO-NPs appeared in the growth and red-shift

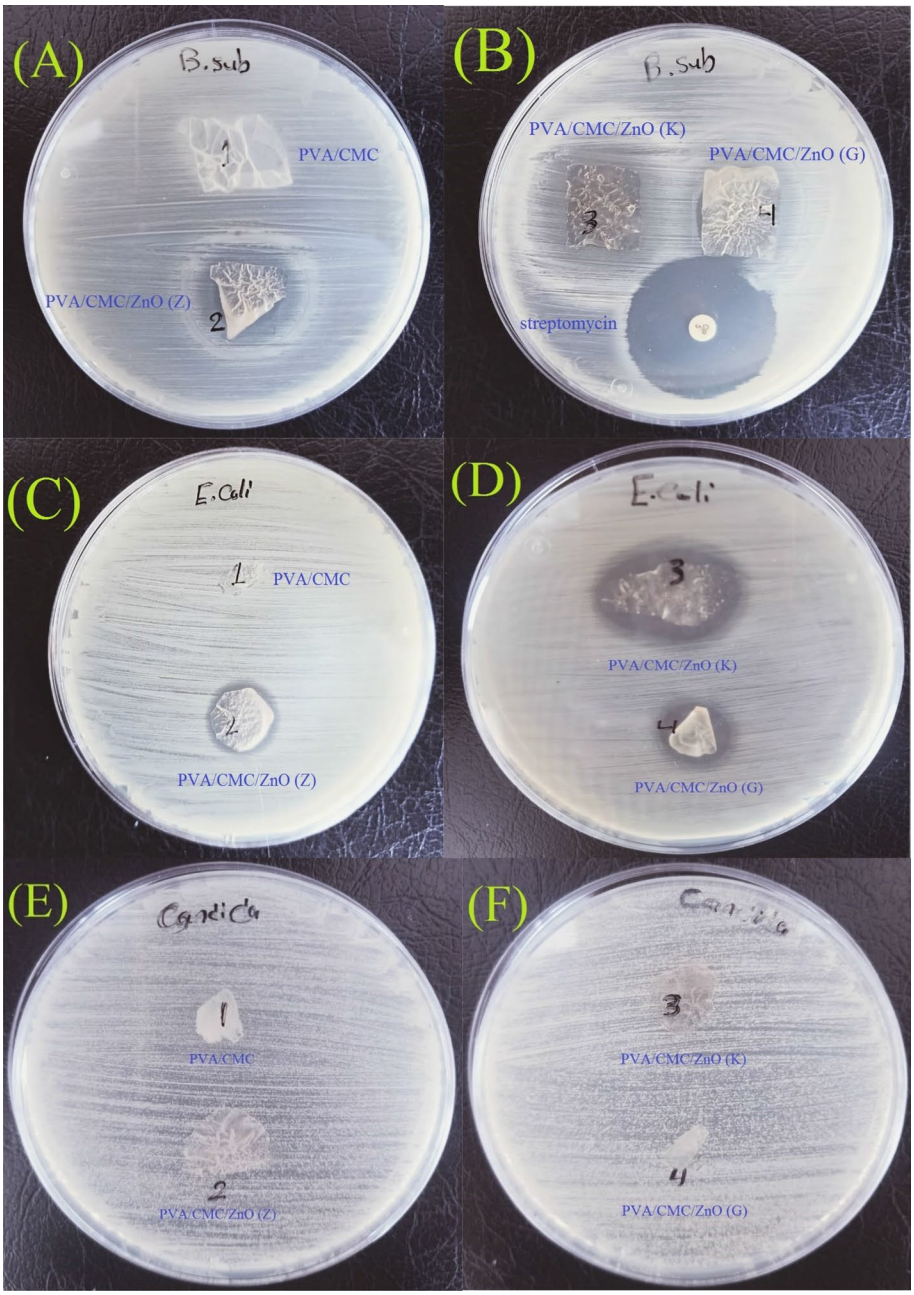


**Fig. 8** Comparison of inhibition zone test between **A**, **B** *Bacillus subtilis*, **C**, **D** *Escherichia coli* and **E**, **F** *Candida albicans* for different samples

**Table 4** Average inhibition zone and approximated efficiency for all prepared samples compared with streptomycin as a positive control

| Microbe | Inhibition zone (mm) | | | | | Approximated efficiency (%) |
|---|---|---|---|---|---|---|
| | A | B | C | D | E | |
| *Bacillus subtilis* | 35 | – | 26 | 33 | 28 | 0, 74, 94 and 80% |
| *Escherichia coli* | 34 | – | 19 | 31 | 23 | 0, 56, 91 and 68% |
| *Candida albicans* | 27 | – | – | – | – | 0, 0, 0, 0% |

(A) Streptomycin as a positive control, (B) CMC/PVA, (C) PCZ-Z, (D) PCZ-K, (E) PCZ-G

of the UV region, which is ascribed to the intermolecular interaction between the hydrogen bonds. The XRD analysis revealed the semi-crystalline nature of the CMC/PVA blend, which decreased after filling with ZnO-NPs. TEM images confirm the presence of ZnO-NPs with a spherical shape and a diameter between 10 and 40 nm. TEM images also

revealed that the CMC/PVA blend is an effective host matrix for the encapsulation of ZnO-NPs, acting as a good capping agent and giving it environmental and chemical stability. All these data support the idea of complexation between ZnO-NPs and polymer matrix. Antibacterial tests revealed that all samples containing ZnO-NPs had exceptional antibacterial activity and were lethal to the bacteria tested. The PCZ-K sample, in particular, displays a high antibacterial efficiency against *E. coli* (91.17%) and *B. subtilis* (94.28%).

**Author Contributions** AYY: resources, data curation, methodology, validation, formal analysis, investigation, conceptualization, supervision, software, visualization, writing—original draft, writing—review & editing. AMA: resources, methodology, formal analysis. RSS: data curation, methodology, validation, formal analysis, investigation, conceptualization, writing—original draft, writing—review & editing. AET: data curation, methodology, validation, formal analysis, investigation, conceptualization, software, visualization, writing—original draft.

**Funding** Open access funding provided by The Science, Technology & Innovation Funding Authority (STDF) in cooperation with The Egyptian Knowledge Bank (EKB). The authors have not disclosed any funding.

## Declarations

**Conflict of interest** The authors declare that we have no known competing financial interests or personal relationships that could have appeared to influence the work reported in this paper.



## References

1. K.S. Siddiqi, A. ur Rahman, Tajuddin, A. Husen, Properties of zinc oxide nanoparticles and their activity against microbes. Nanoscale Res. Lett. **13**, 141 (2018)
2. M. Ikram, A. Haider, M. Imran, J. Haider, S. Naz, A. Ul-Hamid, A. Shahzadi, K. Ghazanfar, W. Nabgan, S. Moeen, S. Ali, Assessment of catalytic, antimicrobial and molecular docking analysis of starch-grafted polyacrylic acid doped BaO nanoparticles. Int. J. Biol. Macromol. **230**, 123190 (2023). https://doi.org/10.1016/j.ijbiomac.2023.123190
3. V.A. Spirescu, C. Chircov, A.M. Grumezescu, B.Ş Vasile, E. Andronescu, Inorganic nanoparticles and composite films for antimicrobial therapies. Int. J. Mol. Sci. **22**, 4595 (2021)
4. S. Moeen, M. Ikram, A. Haider, J. Haider, A. Ul-Hamid, W. Nabgan, T. Shujah, M. Naz, I. Shahzadi, Comparative study of sonophotocatalytic, photocatalytic, and catalytic activities of magnesium and chitosan-doped tin oxide quantum dots. ACS Omega **7**, 46428–46439 (2022). https://doi.org/10.1021/acsomega.2c05133
5. M. Ikram, A. Haider, M. Imran, J. Haider, S. Naz, A. Ul-Hamid, A. Shahzadi, S. Moeen, G. Nazir, W. Nabgan, A. Bashir, Cellulose grafted poly acrylic acid doped manganese oxide nanorods as novel platform for catalytic, antibacterial activity and molecular docking analysis. Surf. Interfaces **37**, 102710 (2023). https://doi.org/10.1016/j.surfin.2023.102710
6. E.E. Elemike, D.C. Onwudiwe, M. Singh, Eco-friendly synthesis of copper oxide, zinc oxide and copper oxide–zinc oxide nanocomposites, and their anticancer applications. J. Inorg. Organomet. Polym. Mater. **30**, 400–409 (2020). https://doi.org/10.1007/s10904-019-01198-w
7. J. Pulit-Prociak, K. Pszczółka, J. Chwastowski, P. Staroń, A. Staroń, E. Sikora, S. Michałowski, M. Banach, Preparation of PVA-based composites with the addition of zinc oxide nanoparticles. J. Inorg. Organomet. Polym. Mater. **29**, 390–401 (2019). https://doi.org/10.1007/s10904-018-1009-2
8. A.E. Tarabiah, H.A. Alhadlaq, Z.M. Alaizeri, A.A.A. Ahmed, G.M. Asnag, M. Ahamed, Enhanced structural, optical, electrical properties and antibacterial activity of PEO/CMC doped ZnO nanorods for energy storage and food packaging applications. J. Polym. Res. **29**, 167 (2022)
9. S. Lopes, F. Ribeiro, J. Wojnarowicz, W. Łojkowski, K. Jurkschat, A. Crossley, A.M.V.M. Soares, S. Loureiro, Zinc oxide nanoparticles toxicity to Daphnia magna: size-dependent effects and dissolution. Environ. Toxicol. Chem. **33**, 190–198 (2014)
10. M. Carofiglio, S. Barui, V. Cauda, M. Laurenti, Doped zinc oxide nanoparticles: synthesis, characterization and potential use in nanomedicine. Appl. Sci. **10**, 5194 (2020)
11. M.S. Nadeem, T. Munawar, F. Mukhtar, M.N. Ur Rahman, M. Riaz, F. Iqbal, Enhancement in the photocatalytic and antimicrobial properties of ZnO nanoparticles by structural variations and energy bandgap tuning through Fe and Co co-doping. Ceram. Int. **47**(8), 11109–11121 (2021). https://doi.org/10.1016/j.ceramint.2020.12.234
12. F. Mukhtar, T. Munawar, M.S. Nadeem, M.N. Ur Rehman, S. Batool, M. Hasan, M. Riaz, K. UrRehman, F. Iqbal, Highly efficient tri-phase $TiO_2$–$Y_2O_3$–$V_2O_5$ nanocomposite: structural, optical, photocatalyst, and antibacterial studies. J. Nanostruct. Chem. **12**, 547–564 (2022). https://doi.org/10.1007/s40097-021-00430-9
13. M.S. Nadeem, T. Munawar, F. Mukhtar, S. Batool, M. Hasan, U.A. Akbar, A.S. Hakeem, F. Iqbal, Energy-levels well-matched direct Z-scheme ZnNiNdO/CdS heterojunction for elimination of diverse pollutants from wastewater and microbial disinfection. Environ. Sci. Pollut. Res. **29**(33), 50317–50334 (2022). https://doi.org/10.1007/s11356-022-19271-2
14. S. Gulati, M. Sachdeva, K.K. Bhasin, Capping agents in nanoparticle synthesis: surfactant and solvent system. AIP Conf. Proc. **1953**, 030214 (2018)
15. M. Arefian, M. Hojjati, I. Tajzad, A. Mokhtarzade, M. Mazhar, A. Jamavari, A review of polyvinyl alcohol/carboxymethyl cellulose (PVA/CMC) composites for various applications. J. Compos. Compd. **2**, 69–76 (2020)
16. A.L. Waly, A.M. Abdelghany, A.E. Tarabiah, Study the structure of selenium modified polyethylene oxide/polyvinyl alcohol (PEO/PVA) polymer blend. J. Mater. Res. Technol. **14**, 2962–2969 (2021)
17. E.M. Abdelrazek, A.M. Abdelghany, A.E. Tarabiah, H.M. Zidan, AC conductivity and dielectric characteristics of PVA/

PVP nanocomposite filled with MWCNTs. J. Mater. Sci. Mater. Electron. **30**, 15521–15533 (2019)
18. A.Y. Yassin, Synthesized polymeric nanocomposites with enhanced optical and electrical properties based on gold nanoparticles for optoelectronic applications. J. Mater. Sci. Mater. Electron. **34**(1), 46 (2023)
19. E. Grządka, J. Matusiak, A. Bastrzyk, I. Polowczyk, CMC as a stabiliser of metal oxide suspensions. Cellulose **27**, 2225–2236 (2020)
20. M. Naseer, U. Aslam, B. Khalid, B. Chen, Green route to synthesize zinc oxide nanoparticles using leaf extracts of *Cassia fistula* and *Melia azadarach* and their antibacterial potential. Sci. Rep. **10**, 1–10 (2020)
21. M.S. Usman, M.E. El Zowalaty, K. Shameli, N. Zainuddin, M. Salama, N.A. Ibrahim, Synthesis, characterization, and antimicrobial properties of copper nanoparticles. Int. J. Nanomed. **8**, 4467 (2013)
22. H.M. Zidan, E.M. Abdelrazek, A.M. Abdelghany, A.E. Tarabiah, Characterization and some physical studies of PVA/PVP filled with MWCNTs. J. Mater. Res. Technol. **8**, 904–913 (2019)
23. T. Ji, R. Zhang, X. Dong, D.E. Sameen, S. Ahmed, S. Li, Y. Liu, Effects of ultrasonication time on the properties of polyvinyl alcohol/sodium carboxymethyl cellulose/nano-ZnO/multilayer graphene nanoplatelet composite films. Nanomaterials **10**(9), 1797 (2020). https://doi.org/10.3390/nano10091797
24. A.A. Al-Muntaser, R.A. Pashameah, A. Saeed, R. Alwafi, E. Alzahrani, S.A. AlSubhi, A.Y. Yassin, Boosting the optical, structural, electrical, and dielectric properties of polystyrene using a hybrid GNP/Cu nanofiller: novel nanocomposites for energy storage applications. J. Mater. Sci. Mater. Electron. **34**, 678 (2023). https://doi.org/10.1007/s10854-023-10104-7
25. M.S. Nadeem, T. Munawar, F. Mukhtar, M.N. ur Rahman, M. Riaz, A. Hussain, F. Iqbal, Hydrothermally derived co, Ni co-doped ZnO nanorods; structural, optical, and morphological study. Opt. Mater. **111**, 110606 (2021). https://doi.org/10.1016/j.optmat.2020.110606
26. M.S. Nadeem, T. Munawar, F. Mukhtar, S. Manzoor, K. Mahmood, M.S. Al-Buriahi, K.M. Katubi, M.N. Ashiq, I. Boukhris, F. Iqbal, Facile synthesis of sunlight driven photocatalysts $Zn_{0.9}Ho_{0.05}M_{0.05}O$ (M= Pr, Sm, Er) for the removal of synthetic dyes from wastewater. Surf. Interfaces **34**, 102376 (2022). https://doi.org/10.1016/j.surfin.2022.102376
27. M. Ikram, A. Haider, S.T. Bibi, A. Ul-Hamid, J. Haider, I. Shahzadi, W. Nabgan, S. Moeen, S. Ali, S. Goumri-Said, M.B. Kanoun, Synthesis of Al/starch co-doped in CaO nanoparticles for enhanced catalytic and antimicrobial activities: experimental and DFT approaches. RSC Adv. **12**(50), 32142–32155 (2022). https://doi.org/10.1039/D2RA06340A
28. R.S. Salama, S.M. El-Bahy, M.A. Mannaa, Sulfamic acid supported on mesoporous MCM-41 as a novel, efficient and reusable heterogenous solid acid catalyst for synthesis of xanthene, dihydropyrimidinone and coumarin derivatives. Colloids Surf. A **628**, 127261 (2021)
29. A.A. Ibrahim, R.S. Salama, S.A. El-Hakam, A.S. Khder, A.I. Ahmed, Synthesis of 12-tungestophosphoric acid supported on Zr/MCM-41 composite with excellent heterogeneous catalyst and promising adsorbent of methylene blue. Colloids Surf. A **631**, 127753 (2021)
30. F.T. Alshorifi, A.A. Alswat, M.A. Mannaa, M.T. Alotaibi, S.M. El-Bahy, R.S. Salama, Facile and green synthesis of silver quantum dots immobilized onto a polymeric CTS–PEO blend for the photocatalytic degradation of p-nitrophenol. ACS Omega **6**, 30432–30441 (2021)
31. A.Y. Yassin, Impedance, structural and thermal analyses of polyvinyl alcohol/polyvinyl pyrrolidone blend incorporated with $Li^+$ ions for lithium-ion batteries. J. Mater. Res. Technol. **15**, 754–767 (2021)
32. M.M. Coleman, D.J. Skrovanek, J. Hu, P.C. Painter, Hydrogen bonding in polymer blends. 1. FTIR studies of urethane-ether blends. Macromolecules **21**, 59–65 (1988)
33. M.A. Mannaa, H.M. Altass, R.S. Salama, MCM-41 grafted with citric acid: the role of carboxylic groups in enhancing the synthesis of xanthenes and removal of heavy metal ions. Environ. Nanotechnol. Monit. Manag. **15**, 100410 (2021)
34. J.C. Cuevas, J. Heurich, F. Pauly, W. Wenzel, G. Schön, Theoretical description of the electrical conduction in atomic and molecular junctions. Nanotechnology **14**, R29–R38 (2003)
35. A.S. Samsudin, M.I.N. Isa, Structural and ionic transport study on CMC doped $NH_4Br$: a new types of biopolymer electrolytes. J. Appl. Sci. **12**, 174–179 (2012)
36. M.A. Saadiah, D. Zhang, Y. Nagao, S.K. Muzakir, A.S. Samsudin, Reducing crystallinity on thin film based CMC/PVA hybrid polymer for application as a host in polymer electrolytes. J. Non-Cryst. Solids **511**, 201–211 (2019)
37. A.Y. Yassin, A.M. Abdelghany, M.M. Shaban, Y.M. Abdallah, Synthesis, characterization and electrochemical behavior for API 5L X70 carbon steel in 5% sulfamic acid medium using PVVH/PEMA blend filled with gold nanoparticles. Colloids Surf. A **635**, 128115 (2022)
38. D. Fink, *Fundamentals of Ion-Irradiated Polymers* (Springer, Heidelberg, 2004)
39. A.M. Salem, A.R. Mohamed, A.M. Abdelghany, A.Y. Yassin, Effect of Polypyrrole on structural, optical and thermal properties of CMC-based blends for optoelectronic applications. Opt. Mater. **134**, 113128 (2022)
40. A.Y. Yassin, A.R. Mohamed, E.M. Abdelrazek, M.A. Morsi, A.M. Abdelghany, Structural investigation and enhancement of optical, electrical and thermal properties of Poly(vinyl chloride-co-vinyl acetate-co-2-hydroxypropyl acrylate)/graphene oxide nanocomposites. J. Mater. Res. Technol. **8**, 1111–1120 (2019)
41. R. Murri, L. Schiavulli, N. Pinto, T. Ligonzo, Urbach tail in amorphous gallium arsenide films. J. Non-Cryst. Solids **139**, 60–66 (1992)
42. L. Zhang, Y. Jiang, Y. Ding, M. Povey, D. York, Investigation into the antibacterial behaviour of suspensions of ZnO nanoparticles (ZnO nanofluids). J. Nanoparticle Res. **9**, 479–489 (2007)
43. K.R. Raghupathi, R.T. Koodali, A.C. Manna, Size-dependent bacterial growth inhibition and mechanism of antibacterial activity of zinc oxide nanoparticles. Langmuir **27**(7), 4020–4028 (2011)
44. O. Bondarenko, K. Juganson, A. Ivask, K. Kasemets, M. Mortimer, A. Kahru, Toxicity of Ag, CuO and ZnO nanoparticles to selected environmentally relevant test organisms and mammalian cells in vitro: a critical review. Arch. Toxicol. **87**, 1181–1200 (2013)
45. A.A. Alswat, M.B. Ahmad, T.A. Saleh, M.Z.B. Hussein, N.A. Ibrahim, Effect of zinc oxide amounts on the properties and antibacterial activities of zeolite/zinc oxide nanocomposite. Mater. Sci. Eng. C **68**, 505–511 (2016)
46. R. Wahab, Y.S. Kim, A. Mishra, S.I. Yun, H.S. Shin, Formation of ZnO micro-flowers prepared via solution process and their antibacterial activity. Nanoscale Res. Lett. **5**(10), 1675–1681 (2010)
47. P.K. Stoimenov, R.L. Klinger, G.L. Marchin, K.J. Klabunde, Metal oxide nanoparticles as bactericidal agents. Langmuir **18**, 6679–6686 (2002). https://doi.org/10.1021/la0202374
48. A. Sirelkhatim, S. Mahmud, A. Seeni, N.H.M. Kaus, L.C. Ann, S.K.M. Bakhori, H. Hasan, D. Mohamad, Review on zinc oxide nanoparticles: antibacterial activity and toxicity mechanism. Nano-Micro Lett. **7**, 219–242 (2015). https://doi.org/10.1007/s40820-015-0040-x
49. F. Mukhtar, T. Munawar, M.S. Nadeem, M.N. Ur Rehman, S.A. Khan, M. Koc, S. Batool, M. Hasan, F. Iqbal, Dual Z-scheme core–shell PANI-$CeO_2$–$Fe_2O_3$–NiO heterostructured nanocomposite for dyes remediation under sunlight and bacterial disinfection. Environ.

Res. **215**, 114140 (2022). https://doi.org/10.1016/j.envres.2022.114140

50. T. Munawar, M.S. Nadeem, F. Mukhtar, M.N. Ur Rehman, M. Riaz, S. Batool, M. Hasan, F. Iqbal, Transition metal-doped $SnO_2$ and graphene oxide (GO) supported nanocomposites as efficient photocatalysts and antibacterial agents. Environ. Sci. Pollut. Res. **29**(60), 90995–91016 (2022). https://doi.org/10.1007/s11356-022-22144-3